

Ferromagnetism in the Periodic Anderson Model

A Comparison of Spectral Density Approximation (SDA), Modified Alloy Analogy (MAA) and Modified Perturbation Theory (MPT)

D. Meyer and W. Nolting

Institut für Physik, Humboldt-Universität zu Berlin, Germany

Received: November 3, 2018

Abstract. We compare different approximation schemes for investigating ferromagnetism in the periodic Anderson model. The use of several approximations allows for a detailed analysis of the implications of the respective methods, and also of the mechanisms driving the ferromagnetic transition. For the Kondo limit, our results confirm a previously proposed mechanism leading to ferromagnetic order, namely an RKKY exchange mediated via the formation of Kondo screening clouds in the conduction band. The contrary case is found in the intermediate-valence regime. Here, the bandshift correction ensuring a correct high-energy expansion of the self-energy is essential. Inclusion of damping effects reduces stability of the ferromagnetic phase.

PACS. 71.10.Fd Lattice fermion models (Hubbard model, etc.) – 71.28.+d Narrow-band systems; intermediate-valence solids – 75.30.Mb Valence fluctuation, Kondo lattice, and heavy-fermion

1 Introduction

The periodic Anderson model (PAM) provides probably the simplest starting point to investigate the interplay between the hybridization of a periodic array of localized (f -) electron levels and a band of itinerant electrons, the strong correlation of the localized electrons and quantum mechanics (Pauli principle)[1].

Within this model, we will investigate the many-body problem of ferromagnetic ordering. Ferromagnetism in the PAM has previously been examined, but most efforts were aimed solely at the so-called Kondo regime of the model. This is defined by an integer number of f -electrons per lattice site. These localized electrons can form an array of well-defined local moments. Via an RKKY interaction, these can order ferro- or antiferromagnetically[2,3,4,5].

In previous papers, we have shown that in the intermediate-valence regime of the PAM, defined by a non-integer filling of the localized levels accompanied by a larger effective hybridization, ferromagnetic order is also possible[6,7,8,9]. This, however, raises some questions concerning the driving mechanism for the ferromagnetic ordering. First of all, in the intermediate-valence regime, quantum fluctuations effectively delocalize the f -electrons, thus the formation of stable moments needs further explanation. A second question is due to the fact, that some of the methods used in the above-mentioned papers, exclude by construction such effects as RKKY as we will discuss below. So why can these methods give meaningful results when neglecting something con-

sidered as essential as RKKY exchange? What should be the driving force towards ferromagnetic ordering in the intermediate valence regime? In this paper, we try to clarify the apparent incoherence of the investigations of ferromagnetism in the PAM in the Kondo and the intermediate-valence regime.

After introducing the model in section 2.1, we will discuss several well-known properties of the system in section 2.2 and finally, in section 2.3, introduce a number of approximation schemes. By comparing to the known properties discussed before, the advantages and disadvantages of these methods will become clear. In section 3, we present and compare results obtained with the different methods. Knowing the strengths and shortcomings of them will help us to understand the origin of ferromagnetic order. Altogether, this will lead us to the conclusion that there are indeed two distinct mechanisms at work: in the Kondo regime, an RKKY exchange has to be seen as the cause of the ferromagnetic order. In the intermediate-valence regime, however, the situation resembles more that of a band-ferromagnet as described by the single-band Hubbard model. In section 4, we will conclude with a summary of our findings.

2 Theory

2.1 The Periodic Anderson Model

We investigate the standard form of the periodic Anderson model (PAM) where a non-degenerate localized f -level

hybridizes with a non-degenerate conduction band (“s-band”) via an on-site hybridization:

$$H = \sum_{\mathbf{k},\sigma} (\epsilon(\mathbf{k}) - \mu) s_{\mathbf{k}\sigma}^\dagger s_{\mathbf{k}\sigma} + \sum_{i,\sigma} (e_f - \mu) f_{i\sigma}^\dagger f_{i\sigma} + \quad (1)$$

$$V \sum_{i,\sigma} (f_{i\sigma}^\dagger s_{i\sigma} + s_{i\sigma}^\dagger f_{i\sigma}) + \frac{1}{2} U \sum_{i,\sigma} n_{i\sigma}^{(f)} n_{i-\sigma}^{(f)}$$

Here, $s_{\mathbf{k}\sigma}$ ($f_{i\sigma}$) and $s_{\mathbf{k}\sigma}^\dagger$ ($f_{i\sigma}^\dagger$) are the creation and annihilation operators for a conduction electron with Bloch vector \mathbf{k} and spin σ (a localized electron on site i and spin σ) and $n_{i\sigma}^{(f)} = f_{i\sigma}^\dagger f_{i\sigma}$. $s_{\mathbf{k}\sigma} = \frac{1}{N} \sum_{\mathbf{k}} e^{i\mathbf{k}\cdot\mathbf{R}_i} s_{i\sigma}$ and $\epsilon(\mathbf{k})$ is the dispersion of the conduction band and e_f is the position of the localized level. The hybridization strength V is taken to be \mathbf{k} -independent, and finally, U is the on-site Coulomb interaction strength between two f -electrons. Throughout this paper, the conduction band will be described by a Bloch (free) density of states, $\rho_0(E) = \frac{1}{N} \sum_{\mathbf{k}} \delta(E - \epsilon(\mathbf{k}))$, of semi-elliptic shape. Its width $W = 1$ sets the energy scale, and its center of gravity the energy-zero: $T_{ii} = \frac{1}{N} \sum_{\mathbf{k}} \epsilon(\mathbf{k}) \stackrel{!}{=} 0$.

The problem of determining the relevant (Zubarev) Green functions[10,11],

$$G_{ij\sigma}^{(f)}(E) = \langle\langle f_{i\sigma}; f_{j\sigma}^\dagger \rangle\rangle; \quad G_{ij\sigma}^{(s)}(E) = \langle\langle s_{i\sigma}; s_{j\sigma}^\dagger \rangle\rangle \quad (2)$$

$$G_{\mathbf{k}\sigma}^{(f,s)} = \frac{1}{N} \sum_{\mathbf{k}} e^{i\mathbf{k}\cdot(\mathbf{R}_i - \mathbf{R}_j)} G_{ij\sigma}^{(f,s)}(E) \quad (3)$$

can be reduced to the *a priori* unknown self-energy via the formal solution of the respective equations of motion:

$$G_{\mathbf{k}\sigma}^{(s)}(E) = \frac{E - (e_f - \mu) - \Sigma_{\mathbf{k}\sigma}(E)}{(E - (e_f - \mu) - \Sigma_{\mathbf{k}\sigma}(E))(E - (\epsilon(\mathbf{k}) - \mu)) - V^2} \quad (4a)$$

$$G_{\mathbf{k}\sigma}^{(f)}(E) = \frac{1}{E - (e_f - \mu) - \frac{V^2}{E - (\epsilon(\mathbf{k}) - \mu)} - \Sigma_{\mathbf{k}\sigma}(E)} \quad (4b)$$

Here, the self-energy is defined by

$$\Sigma_{\mathbf{k}\sigma}(E) G_{\mathbf{k}\sigma}^{(f)}(E) = U \frac{1}{N} \sum_{\mathbf{p},\mathbf{q}} \langle\langle f_{\mathbf{p}-\sigma}^\dagger f_{\mathbf{q}-\sigma} f_{\mathbf{p}+\mathbf{k}-\mathbf{q}\sigma}; f_{\mathbf{k}\sigma}^\dagger \rangle\rangle \quad (5)$$

Throughout this paper, we will apply the local approximation, i. e. assume a \mathbf{k} -independent self-energy. Although becoming exact only in the limit of infinite spatial dimensions, it was shown that this approximation gives satisfactory results already for three dimensions[12,13].

From the Green functions (4a) and (4b), the f - and s -quasiparticle densities of states (f - and s -DOS) can be calculated:

$$\rho_\sigma^{(s)}(E) = -\frac{1}{\pi N} \sum_{\mathbf{k}} \Im G_{\mathbf{k}\sigma}^{(s)}(E - \mu + i0^+) \quad (6a)$$

$$\rho_\sigma^{(f)}(E) = -\frac{1}{\pi N} \sum_{\mathbf{k}} \Im G_{\mathbf{k}\sigma}^{(f)}(E - \mu + i0^+) \quad (6b)$$

The spin-dependent average occupation number $n_\sigma^{(s,f)}$ can now easily be determined:

$$n_\sigma^{(s)} = \langle s_{i\sigma}^\dagger s_{i\sigma} \rangle = \int_{-\infty}^{+\infty} dE f_-(E) \rho_\sigma^{(s)}(E) \quad (7a)$$

$$n_\sigma^{(f)} = \langle f_{i\sigma}^\dagger f_{i\sigma} \rangle = \int_{-\infty}^{+\infty} dE f_-(E) \rho_\sigma^{(f)}(E) \quad (7b)$$

Here, $f_-(E)$ denotes the Fermi function and $\Im x$ the imaginary part of x .

Before introducing our approximative methods, let us discuss some general properties of the PAM.

2.2 General Properties

2.2.1 The Hybridization-Free Case

For vanishing hybridization strength V (“atomic limit”), the problem reduces to that of the zero-bandwidth Hubbard model[14,11]. One obtains for the f -Greenfunction:

$$G_\sigma^{(f,\text{at.})} = \frac{E - (e_f - \mu) - U(1 - n_\sigma^{(f)})}{(E - (e_f - \mu))(E - (e_f - \mu) - U)} \quad (8)$$

with the respective self-energy:

$$\Sigma_\sigma^{(\text{at.})}(E) = \frac{U n_\sigma^{(f)}(E - (e_f - \mu))}{E - (e_f - \mu) - U(1 - n_\sigma^{(f)})} \quad (9)$$

The excitation spectrum consists of two peaks located at e_f and $e_f + U$, which are called *charge excitations*. The conduction band DOS remains unchanged.

2.2.2 The Non-Interacting Limit

The second trivial limit, the interaction-free limit ($U = 0$), yields the following f -Green function:

$$G_{\mathbf{k}\sigma}^{(f,U=0)}(E) = \frac{1}{E - (e_f - \mu) - \frac{V^2}{E - (\epsilon(\mathbf{k}) - \mu)}} \quad (10)$$

The DOS now consists of two features, one corresponding to the f -level, which becomes broadened due to the hybridization. The other feature is the renormalized conduction band. Due to the hybridization there is also an admixture of f -spectral weight into the conduction band region and vice versa. The amount of this admixture of f - and s -states can be understood as a rough estimate of the effective hybridization. It is generally stronger for e_f close to, or inside the conduction band as for e_f well below the band. A further effect is clearly visible when e_f lies within the conduction band. Level-repulsion between f -level and the conduction band induces a gap located approximately at e_f . For e_f below the conduction band, the level repulsion appears only in form of a small shift of the lower edge of the conduction band and the center of the f -level is situated slightly below e_f .

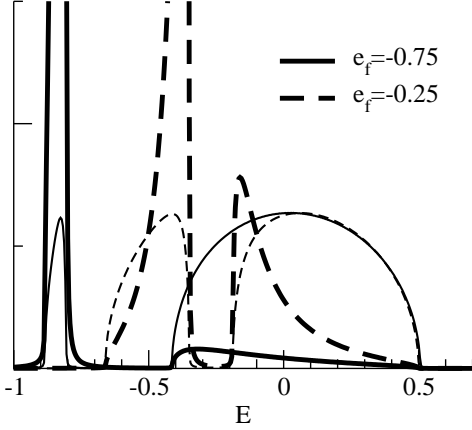


Fig. 1. Density of states for $V = 0.2$, $e_f = -0.75$ and -0.25 in the interaction-free limit ($U = 0$). Thick lines: f -contribution, thin lines conduction band contribution.

These two situations are clearly distinct, one expects different findings in each. The situation of e_f well below the conduction band leads for finite (large) U to the Kondo regime of the PAM. Here the f -level is almost integer-filled. The opposite case, with e_f located within the band and a hybridization strong enough to lead to non-integer $n^{(f)}$, is called intermediate-valence regime. Both situations are plotted in figure 1.

2.2.3 High-Energy Expansion

Next, we introduce a useful high-energy expansion for the f -electron Green function and the self-energy:

$$G_{\mathbf{k}\sigma}^{(f)}(E) = \int dE' \frac{S_{\mathbf{k}\sigma}(E')}{E - E'} = \sum_{n=0}^{\infty} \frac{M_{\mathbf{k}\sigma}^{(n)}}{E^{n+1}} \quad (11)$$

$$\Sigma_{\mathbf{k}\sigma}(E) = \sum_{n=0}^{\infty} \frac{C_{\mathbf{k}\sigma}^{(n)}}{E^n}$$

$S_{\mathbf{k}\sigma}(E) = -\frac{1}{\pi} \Im G_{\mathbf{k}\sigma}^{(f)}(E)$ is the spectral density. Its moments, which are the coefficients of the high-energy expansion of $G_{\mathbf{k}\sigma}^{(f)}(E)$, are defined by

$$M_{\mathbf{k}\sigma}^{(n)} = \int dE E^n S_{\mathbf{k}\sigma}(E); \quad n = 0, 1, 2, \dots \quad (12)$$

and can be calculated independently via

$$M_{\mathbf{k}\sigma}^{(n)} = \langle \underbrace{[\dots [f_{\mathbf{k}\sigma}, H]_-, \dots, H]_-}_{n\text{-fold commutator}}, f_{\mathbf{k}\sigma}^\dagger \rangle_+ \quad (13)$$

where $[\dots, \dots]_-$ denotes the commutator and $[\dots, \dots]_+$ the anti-commutator. By inserting (11) into (4b), one can determine the coefficients of the self-energy expansion.

For the approximative approaches presented below, we only need the local moments $M_{\sigma}^{(n)} = \frac{1}{N} \sum_{\mathbf{k}} M_{\mathbf{k}\sigma}^{(n)}$ and

coefficients $C_{\sigma}^{(n)} = \frac{1}{N} \sum_{\mathbf{k}} C_{\mathbf{k}\sigma}^{(n)}$:

$$M_{\sigma}^{(0)} = 1 \quad (14a)$$

$$M_{\sigma}^{(1)} = e_f + U n_{-\sigma}^{(f)} \quad (14b)$$

$$M_{\sigma}^{(2)} = e_f^2 + 2e_f U n_{-\sigma}^{(f)} + U^2 n_{-\sigma}^{(f)} + V^2 \quad (14c)$$

$$M_{\sigma}^{(3)} = e_f^3 + 3e_f^2 U n_{-\sigma}^{(f)} + U^2 e_f (2n_{-\sigma}^{(f)} + n_{-\sigma}^{(f)2}) + U^3 n_{-\sigma}^{(f)} + V^2 (2e_f + 2U n_{-\sigma}^{(f)} + T_{ii}) + U^2 n_{-\sigma}^{(f)} (1 - n_{-\sigma}^{(f)}) B_{-\sigma} \quad (14d)$$

and

$$C_{\sigma}^{(0)} = U n_{-\sigma}^{(f)} \quad (15a)$$

$$C_{\sigma}^{(1)} = U^2 n_{-\sigma}^{(f)} (1 - n_{-\sigma}^{(f)}) \quad (15b)$$

$$C_{\sigma}^{(2)} = U^2 n_{-\sigma}^{(f)} (1 - n_{-\sigma}^{(f)}) (B_{-\sigma} + U(1 - n_{-\sigma}^{(f)})) \quad (15c)$$

The abbreviation $B_{-\sigma}$ in (14) and (15) stands for a higher correlation function called *bandshift*:

$$n_{-\sigma}^{(f)} (1 - n_{-\sigma}^{(f)}) (B_{-\sigma} - e_f) = V \langle f_{i-\sigma}^\dagger s_{i-\sigma} (2n_{i\sigma}^{(f)} - 1) \rangle \quad (16)$$

In spite of the fact that it is a "higher" correlation function it can rigorously be expressed by the Green function (4b) and the self-energy (5)[15]:

$$n_{-\sigma}^{(f)} (1 - n_{-\sigma}^{(f)}) (B_{-\sigma} - e_f) = -\frac{1}{\pi} \Im \int_{-\infty}^{+\infty} dE f_{-\sigma}(E) \left(\frac{2}{U} \Sigma_{\sigma}(E) - 1 \right) \times \left((E - (e_f - \mu) - \Sigma_{\sigma}(E)) G_{ii}^{(f)}(E) - 1 \right) \quad (17)$$

Surprisingly the hybridization V does not explicitly appear in the $C_{\sigma}^{(n)}$. The contributions via the moments (14) are exactly cancelled by those from the term $\frac{V^2}{E - (\epsilon(\mathbf{k}) - \mu)}$ in (4b). From this, one conclusion can already be drawn: The hybridization V enters the calculation only via equation (4b) in combination with the free conduction band dispersion $\epsilon(\mathbf{k})$. Although there are clearly correlation-induced effects in the conduction band (cf. equation (4a)), these do not feed back into the determination of the high-energy features of the self-energy. Any RKKY-like indirect exchange between f -sites driven by correlations (cf. reference [3]), leaves no footprints in the high-energy behaviour of the self-energy. Although this reasoning works only in the local approximation, it does not imply that the local approximation itself suppresses any RKKY exchange (cf. discussion and references in section 2.3.4).

The prominent high-energy features of the PAM are the charge excitations known from the zero-hybridization limit. One can easily check that in this limit the moments (14) and self-energy coefficients (15) are fulfilled since $B_{-\sigma} \rightarrow e_f$. So obviously, the bandshift, and therefore the $n = 3$ -moment take care of a correction of the positions and weights of the charge excitations in the case of finite interaction and hybridization. We will show below that this correction can be decisive for a proper description of ferromagnetism in the PAM.

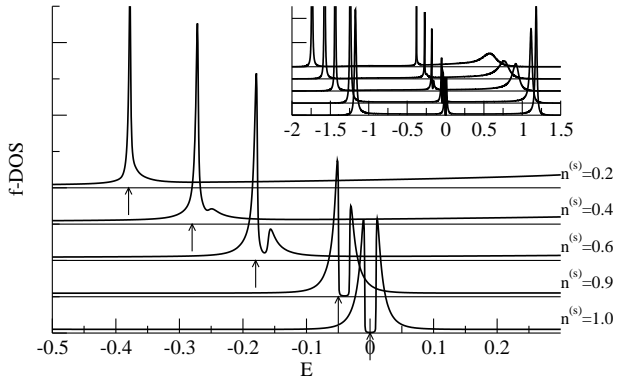


Fig. 2. f -Density of states as obtained within the MPT (see text) for $V = 0.2$, $U = 2$, $n^{(f)} = 1.0$ and different $n^{(s)}$ as indicated. e_f was determined such that $n^{(f)} = 1$ holds. The chemical potential is positioned at the arrows. The inset shows the full energy range, the main picture just the region around μ .

2.2.4 Low-Energy Properties

The PAM is the lattice-periodic extension of the single-impurity Anderson model (SIAM). Since the latter is famous for its special low-energy features (“Kondo-physics”)[1], one expects similar findings also for the PAM. The most prominent finding for the SIAM is the Kondo-screening: At low temperatures, the magnetic moment of the impurity-site is screened by conduction electrons. The remaining conduction electrons form a Fermi liquid. All physical quantities can be scaled by a single energy: the Kondo temperature T_K . In the excitation spectra, the most significant signature of the screening is the occurrence of a sharp resonance at the chemical potential, the *Kondo Resonance*.

The low-energy properties of the PAM have been the subject of intense research[1, 16, 17, 2, 18, 19]. For the symmetric PAM, defined by $n^{(f)} = n^{(s)} = 1.0$ and $e_f = -\frac{U}{2}$, a Kondo resonance appears centered at μ . But contrary to the SIAM, it is split by a gap, the *coherence gap* and the system is insulating. Picturing the Kondo resonance as virtual f -level[20], the gap is simply due to level-repulsion between the “flat band” of the virtual f -levels at every lattice-site and the conduction band. Although it originates from the same mechanism as the gap discussed in section 2.2.2, it is clearly distinguishable: The coherence gap is, together with the Kondo resonance, pinned at μ whereas the hybridization gap discussed in the interaction-free limit would show up at e_f . In figure 2, we present the densities of states as obtained with the below-discussed modified perturbation theory (MPT). Although these DOS are calculated within an approximative method, the qualitatively same picture emerges from the numerically exact Quantum Monte Carlo (QMC)[2, 21] and numerical renormalization group calculations (NRG)[18] and can thus be believed to be qualitatively correct.

The situation of the symmetric PAM is plotted at the bottom of figure 2. Moving away from the symmetric

PAM, e.g. by reducing the number of conduction electrons, the system becomes metallic again. The Kondo resonance gets asymmetric relative to μ , the coherence gap is shifted away from the chemical potential. Further away from the symmetric parameters, the coherence gap closes, which is probably due to quasiparticle damping, since $\Im\Sigma_\sigma(E) \sim E^2$.

A still open question is that of a unique energy scale similar to T_K for the SIAM. The main problem under discussion is the *exhaustion problem* introduced by Nozières[22]. For the case of a periodic array of localized f -levels, the system cannot make available enough conduction electrons to screen all f -moments. This situation is still subject to many investigations[3, 21, 18, 19, 23].

2.3 Approximative Solution of the PAM

In the following sections, we will introduce a series of approximation methods to determine the self-energy (5) of the periodic Anderson model. This series represents a subsequent improvement of the theory along the lines discussed in the last section: The Hubbard-I approximation recovers the non-interacting and the hybridization-free limit but fails to reproduce the high-energy behaviour of the self-energy. This is corrected by the spectral density approximation. This method, however, still suffers from the complete neglect of quasiparticle damping. A straightforward method to incorporate this is the modified alloy analogy. Finally, the low-energy behaviour can be qualitatively reproduced by the modified perturbation theory.

2.3.1 The Hubbard-I Approximation

The first approach presented here is a crude interpolation between the two exactly solvable limiting cases $V = 0$ (cf. section 2.2.1) and $U = 0$ (cf. section 2.2.2). The result equals that of Hubbard’s first work on the Hubbard-model[14], the Hubbard-I approximation.

In the interaction-free limit, one can express the f -Green function (10) in terms of the corresponding $U = 0$ - $V = 0$ (“atomic”) solution:

$$G_{\mathbf{k}\sigma}^{(f,U=0)}(E) = \frac{1}{\left(G_\sigma^{(f,U=0,\text{at.})}(E)\right)^{-1} - \frac{V^2}{E - (\epsilon(\mathbf{k}) - \mu)}} \quad (18)$$

The Hubbard-I approximation is now obtained by assuming the functional dependence of (18) also for the finite- U case. With the atomic-limit Green function for the full PAM (8), this essentially corresponds to inserting the self-energy (9) into equation (4b), therefore

$$\Sigma_\sigma^{(\text{H-I})}(E) = \Sigma_\sigma^{(\text{at.})}(E) = \frac{U n_{-\sigma}^{(f)}(E - (e_f - \mu))}{E - (e_f - \mu) - U(1 - n_{-\sigma}^{(f)})} \quad (19)$$

Although this method is by construction exact in two limiting cases, namely the interaction-free ($U = 0$) and

the hybridization-free ($V = 0$) case, a number of shortcomings follows directly from inspecting equation (19) and its derivation. First of all, the self-energy (19) fulfills the high-energy expansion only up to the $n = 1$ self-energy coefficient. The bandshift correction $B_{-\sigma}$ is neglected. This yields a weak spin-dependence through the expectation values $n_{-\sigma}^{(f)} = \langle n_{i-\sigma}^{(f)} \rangle$ only. Second, the self-energy (19) is real, any quasiparticle damping effects as indicated by a finite imaginary part of $\Sigma_{\sigma}(E)$ are ignored. The third drawback is the suppression of any feedback mechanism from the conduction band: The latter enters the calculation only via equation (18). This implies that although there are correlation-induced changes in the conduction band (cf. equation (4a)), these do not feedback into the f -self-energy (19). An indirect magnetic exchange between the f -electrons via polarization of the conduction band (“RKKY”) cannot appear in this approximation method. Finally, none of the expected low-energy features of the PAM, as discussed in section 2.2.4 can be found using this method.

2.3.2 The Spectral Density Approximation

The spectral density approximation (SDA)[24,11,25] is the result of a direct improvement of the above-discussed Hubbard-I approximation with respect to the high-energy expansion (11).

Starting with an ansatz for the self-energy using the same functional structure as (19),

$$\Sigma_{\sigma}(E) = \alpha_{1\sigma} \frac{E - \alpha_{2\sigma}}{E - \alpha_{3\sigma}} \quad (20)$$

one can fit the coefficients $\alpha_{p\sigma}$ in such a way that the high energy expansion of the self-energy (11) with the coefficients (15) is fulfilled. One readily arrives at

$$\Sigma_{\sigma}^{(\text{SDA})}(E) = \frac{Un_{-\sigma}^{(f)}(E - B_{-\sigma} - (e_f - \mu))}{E - B_{-\sigma} - (e_f - \mu) - U(1 - n_{-\sigma}^{(f)})} \quad (21)$$

The SDA self-energy differs from the Hubbard-I solution by the bandshift $B_{-\sigma}$ (16). It is introduced by the $n = 3$ -moment (14d) and responsible to reproduce the correct high-energy behaviour of the f -Green function. It leads to a (possibly spin-dependent) shift of the positions of the f -peaks in the density of states. So without loosing any of the advantages of the Hubbard-I approximation, as the correct reproduction of the $U = 0$ and the $V = 0$ limits and its numerical simplicity, one major drawback of this method can be removed. However, the other points of criticism, as the missing quasiparticle damping and the incorrect low-energy properties remain.

The name “spectral density approximation” stems from its application to the Hubbard model, where this approach is derived by a physically motivated two-pole ansatz for the spectral density[24,25]. Results for the SDA in the context of the PAM were previously published[6,7]. In these papers, the SDA was applied to a set of effective Hubbard models, onto which the PAM could be mapped.

However, the above-described procedure leads to exactly the same results as those published in references [6,7]

2.3.3 The Modified Alloy Analogy

Now we want to present a method that resolves one major drawback of the already introduced methods: Both the Hubbard-I and the SDA self-energies are real. Quasiparticle damping as represented by a finite imaginary part of the self-energy is therefore completely neglected. A well-known method to incorporate damping effects is the alloy-analogy approach. By using physical intuition or by other justified means, the original problem is mapped onto an fictitious alloy, which subsequently can be solved using standard methods as e. g. the coherent potential approximation (CPA)[26].

The CPA represents the best “single-site” method for solving an alloy-problem[11]. Single-site approximation in this context is equivalent to the already introduced local approximation or \mathbf{k} -independence of the self-energy. The alloy is defined by the energy levels of its components, $E_{p\sigma}$ and their respective concentrations $x_{p\sigma}$, where the index p numbers the components. The corresponding self-energy can be determined by solving the CPA-equation:

$$0 = \sum_{p=1}^n x_{p\sigma} \frac{E_{p\sigma} - \Sigma_{\sigma}(E) - e_f}{1 - G_{ii\sigma}^{(f)}(E)(E_{p\sigma} - \Sigma_{\sigma}(E) - e_f)} \quad (22)$$

In the conventional alloy analogy for the PAM[27,28,29], the artificial alloy is determined by the poles of the atomic limit f -Green function (8) and their respective weights:

$$\begin{aligned} E_{1\sigma}^{(AA)} &= e_f; & x_{1\sigma}^{(AA)} &= 1 - n_{-\sigma}^{(f)} \\ E_{2\sigma}^{(AA)} &= e_f + U; & x_{2\sigma}^{(AA)} &= n_{-\sigma}^{(f)} \end{aligned} \quad (23)$$

This choice, however, is in no way predetermined. In reference [8], another alloy analogy, the modified alloy analogy (MAA) was proposed for the PAM in analogy to the MAA for the Hubbard model[30]: By inserting equation (11) into (22) and comparing the coefficients in $\frac{1}{E}$, an optimum two-component alloy analogy with respect to the high-energy behaviour can be found:

$$\begin{aligned} E_{1,2\sigma} &= \frac{1}{2} [B_{-\sigma} + U + e_f \pm \\ &\quad \sqrt{(B_{-\sigma} + U - e_f)^2 + 4Un_{-\sigma}^{(f)}(e_f - B_{-\sigma})}] \\ x_{1\sigma} &= \frac{E_{2\sigma} - e_f - Un_{-\sigma}^{(f)}}{E_{2\sigma} - E_{1\sigma}} = 1 - x_{2\sigma} \end{aligned} \quad (24)$$

It should be noted that $E_{1,2\sigma}$ coincide with the poles of the SDA Green function (cf. equations (21) and (4b)) when the term $\frac{V^2}{E - (\epsilon(\mathbf{k}) - \mu)}$ in the denominator of the Green function is neglected.

By construction, the MAA fulfills the high-energy expansion (11) up to the $n = 3$ moment or equivalently the $n = 2$ self-energy coefficient (15c). Also, damping effects are considered. However, the MAA still suffers from

the complete neglect of the low-energy properties (cf. section 2.2.4) and the self-energy is determined in such a way that correlation effects within the conduction band do have no influence (“feedback”) onto $\Sigma_\sigma(E)$. A more detailed discussion of the MAA applied to the PAM can be found in reference [8].

2.3.4 The Modified Perturbation Theory

Let us finally introduce the modified perturbation theory. This approach is based on the dynamical mean-field theory (DMFT)[31,32]. In the case of a local self-energy, which becomes exact in the limit of infinite spatial dimensions[33,34], the PAM can be mapped onto a single-impurity Anderson model (SIAM) with the Hamiltonian,

$$H = \sum_{\mathbf{k},\sigma} (\epsilon(\mathbf{k}) - \mu) s_{\mathbf{k}\sigma}^\dagger s_{\mathbf{k}\sigma} + \sum_{\sigma} (e_d - \mu) d_{\sigma}^\dagger d_{\sigma} + \quad (25)$$

$$\sum_{\sigma} V_{\mathbf{k}d} (d_{\sigma}^\dagger s_{\mathbf{k}\sigma} + s_{\mathbf{k}\sigma}^\dagger d_{\sigma}) + \frac{1}{2} U \sum_{\sigma} n_{\sigma}^{(d)} n_{-\sigma}^{(d)}$$

The notation is as for the PAM (cf. equation (1)). $d_{\sigma}^{(\dagger)}$ are the annihilation (creation) operators for electrons at the impurity, its energy level is e_d . In the case of the DMFT, the bath of conduction electrons, usually defined by $\epsilon(\mathbf{k})$ and $V_{\mathbf{k}d}$ need not be specified in detail. For all practical calculations, it is sufficient to know the *hybridization function* $\Delta(E)$, in the pure SIAM defined by $\Delta(E) = \sum_{\mathbf{k}} \frac{V_{\mathbf{k}d}^2}{E - \epsilon(\mathbf{k})}$. However, for the mapping of the DMFT to be successful, the hybridization function has to be determined according to the *self-consistency condition*[32]

$$\Delta_{\sigma}(E) = E - (e_f - \mu) - \Sigma_{\sigma}(E) - \left(G_{ii\sigma}^{(f)}(E)\right)^{-1} \quad (26)$$

This implies that in case of symmetry breaking, the hybridization function becomes spin-dependent. Now one can make use of the fact that the impurity self-energy of the SIAM defined by equation (26) is equivalent to the self-energy of the PAM. The advantage of the mapping is that the SIAM is one of the simplest known many-body models, several exact statements as well as well-tested approximative solutions are known. In the following, we apply the modified perturbation theory, which was explained and discussed in detail elsewhere[35,36,19,9]. So we will restrict ourselves to a short summary of this approach.

Starting point is the following ansatz for the self-energy[37,38,39]:

$$\Sigma_{\sigma}(E) = U \langle n_{-\sigma}^{(f)} \rangle + \frac{\alpha_{\sigma} \Sigma_{\sigma}^{(\text{SOC})}(E)}{1 - \beta_{\sigma} \Sigma_{\sigma}^{(\text{SOC})}(E)} \quad (27)$$

α_{σ} and β_{σ} are introduced as parameters to be determined later. $\Sigma_{\sigma}^{(\text{SOC})}(E)$ is the second-order contribution to perturbation theory around the Hartree-Fock solution[40,41,13]. Equation (27) can be understood as the simplest possible ansatz which can, on the one hand, reproduce the

perturbational result in the limit $U \rightarrow 0$, and, on the other hand, recovers the atomic limit for appropriately chosen α_{σ} and β_{σ} [42].

Using the perturbation theory around the Hartree-Fock solution introduces an ambiguity into the calculation. Within the self-consistent Hartree-Fock calculation, one can either choose the chemical potential to be equivalent to the chemical potential of the full MPT calculation, or take it as parameter $\tilde{\mu}$ to be fitted to another physically motivated constraint. In reference [39] and other papers [43,44], the Luttinger theorem[45] or equivalently the Friedel sum rule[46,47] was used to determine $\tilde{\mu}$. Since these theorems are applicable only for $T = 0$, this limits the calculations to zero temperature. In order to access finite temperatures, we used the condition of identical electron densities for the Hartree-Fock and the full calculation ($n_{\sigma}^{(f,\text{HF})} = n_{\sigma}^{(f)}$). In our view, it is more reasonable to perform the Hartree-Fock calculation for the same electron density rather than identical chemical potential of the full MPT calculation since the electron density is a critical parameter concerning correlation effects. A more detailed analysis of the different possibilities to determine $\tilde{\mu}$ is found in reference [35]. Finally, the parameters α_{σ} and β_{σ} have to be determined. Instead of using the “atomic” limit of $V = 0$ as was done e. g. in references [39,44,48], we make use of the moments of the spectral density. Analogously to equations (11), (13) and (14), these can be evaluated for the SIAM. To fit the two parameters of ansatz (27), the first three self-energy coefficients are needed, since $C_{\sigma}^{(0)}$ is reproduced for any choice of α_{σ} and β_{σ} .

As for the PAM, a bandshift correlation function similar to (16) is introduced via $C_{\sigma}^{(2)}$ and the procedure leads to the correct high-energy behaviour of the Green function for the SIAM and via the DMFT-mapping also for the PAM. So while recovering the main advantage of the SDA and MAA, namely the correct reproduction of the high-energy expansion (11) up to the $n = 3$ -moment, the MPT yields a major improvement concerning the low-energy properties of the PAM. Although already for the SIAM the low-energy scale (“Kondo temperature” T_K) connected with these properties, cannot be quantitatively reproduced, other quantities can, at least in a qualitatively satisfactory way, be recovered[36,19]. In particular, the densities of states both above and below the Kondo temperature, but also the general features of the susceptibility $\chi(T)$ seem to be trustworthy. Another test of the low-energy properties is given by the Friedel sum rule, which links the self-energy at the Fermi energy with the electron density. Within the MPT, it is fulfilled in a large parameter space[36]. It is also worth mentioning that via the DMFT self-consistency (26), a feedback from correlation-induced features in the conduction band onto the f -self-energy is possible. In the limit of infinite spatial dimension ($d \rightarrow \infty$), where the DMFT becomes exact, the RKKY exchange between any two lattice sites will vanish. However, as discussed in reference [2], the net exchange of one lattice site with a shell of neighbors remains finite since the number of sites in the respective shell diverges as $d \rightarrow \infty$.

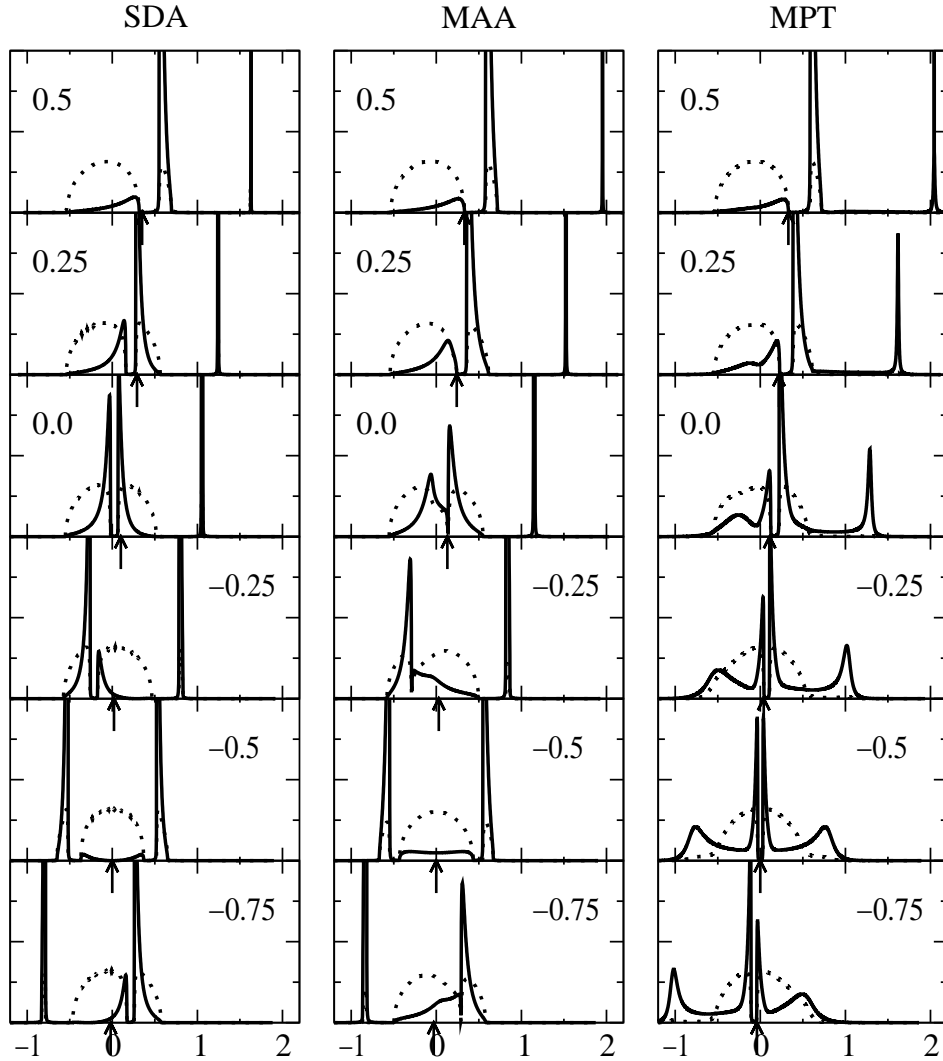


Fig. 3. s -DOS (f -DOS) as dotted (solid) lines for $V = 0.1$, $U = 1$ and $n^{(\text{tot})} = 2.0$. The respective value of e_f is given in each graph. The position of the chemical potential is denoted by the arrows. The left column was calculated with the SDA, the middle within MAA and the right column within MPT.

This exchange is incorporated in the (spin-dependent) hybridization function (26).

3 Results and Discussion

In the following we will present the results obtained with the different approximation schemes of section 2.3 and hope to shed some light on the mechanism that leads to ferromagnetism in the PAM in the Kondo- and intermediate-valence regime. First however, we will look at the paramagnetic quasiparticle densities of states (DOS) as defined by equations (6a) and (6b).

In figure 3, both the f - and s -DOS are plotted for a relatively small interaction strength $U = 1.0$ and $V = 0.2$, $n^{(\text{tot})} = 2.0$ at zero temperature and for various e_f as indicated. The second picture from the bottom represents the above-introduced symmetric case with $e_f = -0.5 =$

$-\frac{U}{2}$. The position of the chemical potential μ is indicated by the arrows. The left column was obtained using the SDA, the middle MAA and the right column by using the MPT.

The SDA DOS differs from the interaction-free case (cf. section 2.2.2) plotted in figure 1 by the appearance of a second charge excitation approximately at $e_f + U$. If either e_f or $e_f + U$ falls within the band region, a hybridization gap as discussed in section 2.2.2 is clearly visible. The Hubbard-I results are not shown in figure 3. These look very similar to the SDA DOS, only a small shift of the charge excitations can be noticed. In the symmetric case they are identical, the bandshift vanishes.

The MAA DOS shows some modifications when compared to the SDA: The quasiparticle damping softens the charge excitations and the hybridization gap is for $e_f \lesssim 0$ almost closed. For $e_f \gtrsim 0.25$ the DOS strongly resembles the SDA results. This can be understood since the num-

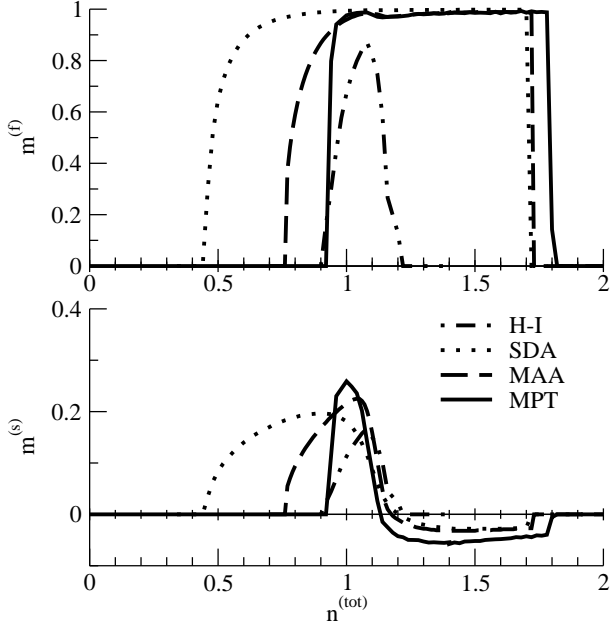


Fig. 4. s - and f - polarization for $U = 4$, $V = 0.1$, $T = 0$ and $e_f = -0.35$ (s : lower, f : upper panel). The results of Hubbard-I, SDA, MAA and MPT are shown. Please note the different scales of the y-axis.

ber of f -electrons, $n^{(f)}$ is very small. Scattering processes become rare and the quasiparticle damping, which differentiates between SDA and MAA, negligible. As in the case of the SDA and Hubbard-I approximation, the simpler theory disrespecting the high-energy expansion and neglecting the bandshift correction, in this case the conventional alloy analogy (23), yields very similar and in the symmetric case identical results. We will see below that the bandshift correction becomes much more important in the ferromagnetic phase.

Finally, the DOS obtained by MPT shows remarkable differences, especially close to the chemical potential. These represent the “Kondo physics” discussed in section 2.2.4. Again, we note that for $e_f \gtrsim 0.25$ the DOS resemble the SDA and MAA results. This is obviously for the same reasons as discussed above, namely the small number of f -electrons.

In figure 4, the f - and s -magnetization is plotted as function of the total electron density $n^{(\text{tot})}$ for $U = 4$, $e_f = -0.35$, $V = 0.1$ and $T = 0$. Within the Hubbard-I approximation, a small region of ferromagnetism is found around $n^{(\text{tot})} \approx 1$. The conduction band magnetization $m^{(s)}$ (thin lines in figure 4) is always positive. We call this situation parallel s - f coupling.

In the SDA the region of ferromagnetism is strongly enlarged. This is a clear indication of the importance of the bandshift correction with respect to ferromagnetism. Since the bandshift (16) can be spin-dependent, it enhances the possibility of ferromagnetic ordering. We also note an interesting behaviour of the conduction band magnetization: as function of electron density, it changes sign. For low

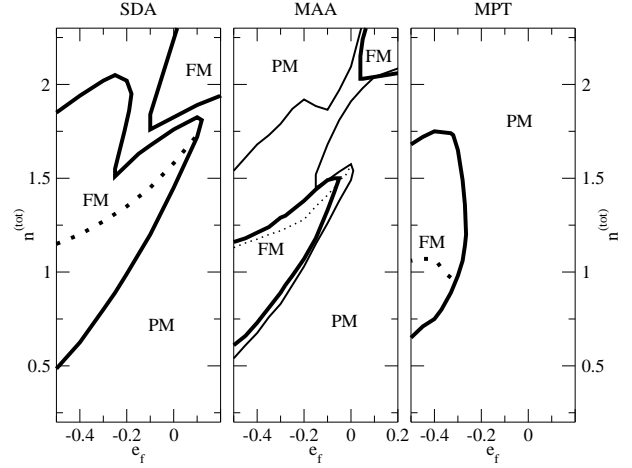


Fig. 5. $T = 0$ phase diagram for the PAM in the intermediate-valence regime with $U = 4$ and $V = 0.2$ as obtained within SDA, MAA and MPT calculations. For the MAA, the phase diagram for $V = 0.1$ is additionally plotted as thin lines. The dotted lines separate the regions of parallel (below the dotted line) and anti-parallel (above) s - f coupling. Note: for the MAA with $V = 0.2$, the low-density ferromagnetic region exhibits only parallel, the high-density region only antiparallel s - f coupling.

$n^{(\text{tot})}$, the s - f coupling is parallel, for higher values antiparallel. This behaviour, which is also found within the MAA and MPT, can be traced back to the appearance of the hybridization gap discussed in section 2.2.2. A more detailed investigation of this can be found in references [9, 8].

The MAA result can be used to estimate the influence of quasiparticle damping. One observes a reduction of the ferromagnetic region compared to the SDA result. So, similar to the Hubbard model[30,49], quasiparticle damping is unfavourable for ferromagnetism. However, apart from the lower critical $n^{(\text{tot})}$, the MAA and SDA curves are very similar. It should be noted that with the conventional alloy analogy (23), no ferromagnetic solution can be found[27]. This confirms again the importance of the bandshift correction (16) with respect to ferromagnetism.

The same holds true for the MPT result. Again, the region of ferromagnetism is reduced as compared to the MAA, but the change is rather small. Qualitative features as the change of sign of the conduction band magnetization, and the generally larger conduction band polarization in case of parallel coupling remain the same for SDA, MAA and MPT. It should further be pointed out that the lower critical $n^{(\text{tot})}$ is, when varying e_f , in fact determined by $n^{(f)}$. The number of conduction band electrons, $n^{(s)}$ plays no significant role[9].

From all these observations we conclude that the bandshift correction has a strong influence on ferromagnetism. So does the inclusion of quasiparticle damping. However, at least in the examined situation of the PAM in the intermediate-valence regime, there seems to be no major difference between the MAA without, and the MPT

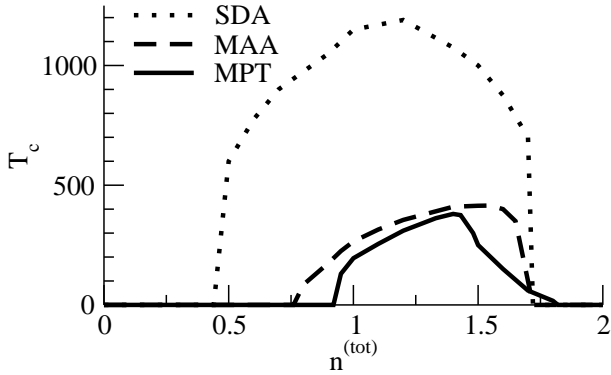


Fig. 6. The Curie temperature as function of total electron density for $U = 4$, $V = 0.1$ and $e_f = -0.35$.

including the special low-energy properties of the PAM. These have apparently less influence on ferromagnetism in the intermediate-valence regime of the PAM.

A quite similar picture emerges from an inspection of the phase diagram in figure 5. A comparison of SDA and MAA results shows the negative influence of quasiparticle damping on ferromagnetism. Furthermore, another important point should be noticed here: in the MAA calculation, a hybridization strength of $V = 0.2$ already strongly reduces the magnetic region compared to the $V = 0.1$ case. It is apparent that only the region with antiparallel s - f coupling is affected by this. The region with parallel s - f coupling remains almost unchanged. It was shown in reference [8] that the MAA shows an anomalous hybridization dependence in this region. Whereas for other electron densities, an increasing hybridization strength V quickly suppresses ferromagnetism[8], here the Curie temperature increases with increasing V after going through a minimum. The same behaviour is found within the SDA. However, the MPT does not show this behaviour at all. As discussed in reference [19], the local moments get quenched by formation of local Kondo singlets with increasing V . Being of low-energy nature, this effect is not covered by the other approximation schemes. The apparent stability of ferromagnetism around $n^{(tot)} \approx 1$ in these methods for large hybridization strengths seems therefore to be rather meaningless.

A further difference between MAA and MPT is the upper critical f -level position e_f . The modifications in the MPT are due to the fact that the lower charge excitation joins with the Kondo resonance. The existence of the latter is neglected in the MAA. The MPT seems to be more reliable for determining this phase boundary.

In figure 6, the Curie temperatures as function of the total electron density are plotted for the same model parameters as used in figure 4. Again the conclusions are consistent: The quasiparticle damping which basically discriminates SDA and MAA, leads to a huge reduction of T_c . The inclusion of the low-energy physics, as done by the MPT, does not change T_c much, only above $n^{(tot)} \approx 1.5$, a suppression of T_c is observed. It is further noteworthy that the change of sign of the conduction band magnetization

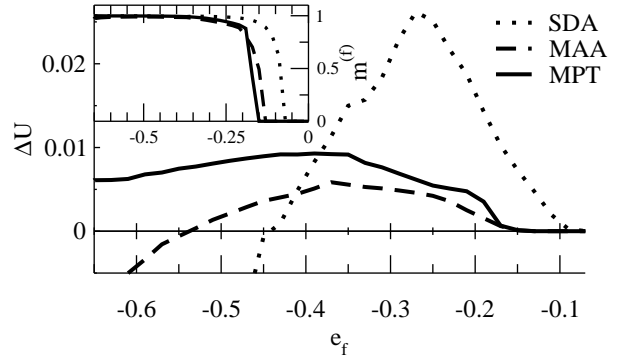


Fig. 7. Difference of the internal energy for the paramagnetic and ferromagnetic solution (see text). The inset shows the f -magnetization of the ferromagnetic solution. All calculations for $U = 4$, $V = 0.1$, $T = 0$ and $n^{(tot)} = 1.2$.

as seen in figure 4 does not lead to any particularity in the T_c curves.

Up to now we have focused on the PAM in the intermediate-valence regime. What happens to the ferromagnetic solution upon entering the Kondo regime? The situation is plotted in figure 7. The inset shows the f -magnetization. All three methods (SDA, MAA and MPT) do have a self-consistent ferromagnetic solution for e_f well below the conduction band. An inspection of the internal energies $\langle H \rangle$, which can be calculated analogously to (7) and (17), of the ferromagnetic and the paramagnetic solution reveals, however, that for the SDA and MAA the ferromagnetic solutions are not the stable ones, the system is in fact paramagnetic. This is not the case for the MPT. Here the ferromagnetic solution remains stable. This indicates that in the Kondo regime, the low-energy properties become much more important concerning ferromagnetic ordering. This was first proposed in reference [3], where the origin of ferromagnetic order in the Kondo regime was identified as RKKY-like. The polarization of the conduction band is due to the formation of Kondo screening clouds[3]. As was already argued in section 2.3, the MAA and the SDA are not able to reproduce such a mechanism whereas the MPT should contain this at least qualitatively.

So whereas in the intermediate-valence regime, the SDA, the MAA and the MPT show similar results, they give completely different pictures in the Kondo regime. This leads us to the conclusion that there have to be two distinct mechanisms driving the ferromagnetic ordering in these two different areas in parameter space. Whereas in the Kondo regime, a RKKY mechanism is doubtless the key factor, as discussed above and in reference [3], the situation is clearly different in the intermediate-valence regime. Here, the correct reproduction of high-energy features, the charge excitation as ensured by the band-shift correction (16) seems crucial. The inclusion of the particular low-energy properties of the PAM does not significantly change the behaviour. From our observations, we are led to propose a single-band mechanism similar to the one leading to ferromagnetism in the single-band

Hubbard model to be responsible for the ferromagnetic ordering in the intermediate-valence regime.

This proposal is further supported by the following observations:

I) The critical interaction strength U_c is much larger in the intermediate-valence regime than in the Kondo regime thus pointing to a genuine strong-coupling effect (cf. reference [9]).

II) The lower critical $n^{(\text{tot})}$ marking the breakdown of ferromagnetism is in fact determined by a critical $n^{(f)}$ [9]. The conduction electron density has no influence on the magnetic phase boundaries. This is a clear reference to a single-band mechanism.

III) The polarization of the conduction band shows a remarkable behaviour as e.g. its change of sign. This, however, does not affect important magnetic quantities as the Curie temperature. The polarization of the conduction electrons seems to be a consequence and not the cause of the ferromagnetic ordering of the f electrons.

From these points, we arrive at the proposition that the ferromagnetic order in the intermediate-valence regime is due to some intra-band mechanism. For the Hubbard model[14,50,51], the existence of a ferromagnetic phase in the strong-coupling regime was confirmed in the limit of infinite dimensions[52,53]. The mechanism driving this transition is simply based on a gain of kinetic energy[54,49]. This is supported by the strong dependency on the shape of the free ($U = 0$) density of states[55,56]. It was confirmed that ferromagnetism is most favored in case of a non-symmetric DOS which has a divergence at or close to one of its edges. Going back to the PAM, we note that the hybridization leads in the intermediate-valence regime to an effective f - f -hopping. The f -electrons form a strongly correlated band. This band fits well into the prerequisites of a single-band ferromagnet as lined out above: The band is narrow, strongly asymmetric and most of its spectral weight is, for appropriate values of e_f , located near its edge (cf. figure 1, thick lines). The proposed similarity between ferromagnetism in the intermediate-valence regime of the PAM and the Hubbard model manifests itself also in the fact that in both cases, the fulfillment of the high-energy expansion (11) (as done by SDA, MAA and MPT) seems crucial for a proper description of the phenomenon[49].

4 Summary

In this paper, we have discussed ferromagnetism in the periodic Anderson model (PAM), and possible mechanisms driving the magnetic ordering.

We have reviewed a series of approximation schemes, from the Hubbard-I, via the spectral-density approximation (SDA) and the modified alloy analogy (MAA) to the modified perturbation theory (MPT). This series represents a subsequent improvement according to several exactly known properties of the model. The Hubbard-I approximation is exact in the two limiting cases of vanishing hybridization ($V = 0$) and interaction ($U = 0$). Its systematic improvement with respect to the correct reproduction

of the high-energy expansion of the self-energy leads directly to the spectral density approximation. The inclusion of quasiparticle damping effects without losing the correct high-energy behaviour is possible via the modified alloy analogy procedure. Finally, the modified perturbation theory still recovers the correct high-energy expansion, includes quasiparticle damping effects, and additionally incorporates, at least qualitatively correct, the special low-energy properties of the PAM.

The results of the SDA, MAA and MPT compare well in the intermediate-valence regime. By comparing with the Hubbard-I approximation, it becomes clear that the correct reproduction of the high-energy behaviour is crucial for a correct description of ferromagnetism in this parameter regime. The influence of quasiparticle damping is, as expected, a reduction of the magnetic stability as indicated by a strongly reduced Curie temperature and smaller ferromagnetic area in the $T = 0$ phase diagram. The low-energy physics seem to have only minor effects on the ferromagnetic properties.

In the Kondo regime, the picture is completely different. Only the MPT yields a stable ferromagnetic phase. This, however, is in agreement with QMC calculations[3]. The SDA and MAA fail to recover these results. The origin of the ferromagnetic ordering in the Kondo regime is an RKKY exchange as discussed in reference [3]. We showed in this paper why the SDA and MAA cannot reproduce such a mechanism.

However, the good qualitative agreement between the SDA, MAA and MPT results in the intermediate-valence regime let us believe that here the driving mechanism towards the ferromagnetic transition must be of different nature. Our results gave some hints that this mechanism is similar to that driving the ferromagnetic ordering in the single-band Hubbard model with a band formed by the effectively delocalized f electrons.

We acknowledge fruitful discussions with our colleagues A. Ramakanth and G. G. Reddy from Kakatiya University, Warangal (India), in the process of adapting the MAA to the periodic Anderson model. This collaboration was financially supported by the *Volkswagen foundation*. One of the authors (D. M.) further acknowledges support from the *Friedrich-Naumann foundation*.

References

1. A. C. Hewson, *The Kondo Problem to Heavy Fermions*, Cambridge University Press 1993.
2. M. Jarrell, Phys. Rev. B **51**(12), 7429 1995.
3. A.N. Tahvildar-Zadeh, M. Jarrell, and J.K. Freericks, Phys. Rev. B **55**(6), R3332 1997.
4. B. Möller and P. Wölfle, Phys. Rev. B **48**(14), 10320 1993.
5. R. Doradziński and J. Spalek, Phys. Rev. B **58**(6), 3293 1998.
6. D. Meyer, W. Nolting, G.G. Reddy, and A. Ramakanth, phys. stat. sol. (b) **208**, 473 1998.
7. D. Meyer and W. Nolting, Physica B **259**, 918 1999.

8. G. G. Reddy, D. Meyer, S. Schwieger, A. Ramakanth, and W. Nolting, *J. Phys: Cond. Mat.* in press.
9. D. Meyer and W. Nolting, *Phys. Rev. B* **62**(9), 5657 2000.
10. D.N. Zubarev, *Sov. Phys. Usp.* **3**(3), 320 1960.
11. W. Nolting, *Viel-Teilchen-Theorie* volume 7 of *Grundkurs: Theoretische Physik*, Friedr. Vieweg & Sohn Verlagsgesellschaft mbH Braunschweig/Wiesbaden 3 edition 1997.
12. H. Schweizer and G. Czycholl, *Solid State Commun.* **69**(2), 171 1989.
13. H. Schweitzer and G. Czycholl, *Solid State Commun.* **74**(8), 735 1990.
14. J. Hubbard, *Proc. R. Soc. London, Ser. A* **276**, 238 1963.
15. G. Geipel and W. Nolting, *Phys. Rev. B* **38**, 2608 1988.
16. R. M. Fye, *Phys. Rev. B* **41**(4), 2490 1990.
17. N. Grewe and F. Steglich, In K. A. Gschneidner and L. Eyring, editors, *Handbook on the Physics and Chemistry of Rare Earth* volume 14 page 343. Elsevier Science Publishers Amsterdam 1991.
18. T. Pruschke, R. Bulla, and M. Jarrell, *Phys. Rev. B* **61**(19), 12799 2000.
19. D. Meyer and W. Nolting, *Phys. Rev. B* **61**(20), 13465 2000.
20. P. W. Anderson, *Phys. Rev.* **124**(1), 41 1961.
21. A.N. Tahvildar-Zadeh, M. Jarrell, and J.K. Freericks, *Phys. Rev. Lett.* **80**(23), 5168 1998.
22. P. Nozières, *Eur. Phys. J. B* **6**, 447 1998.
23. S. Burding, A. Georges, and D. R. Grempel, *cond-mat/0004043*.
24. W. Nolting, *Phys. Lett.* **38A**, 417 1972.
25. T. Herrmann and W. Nolting, *J. Magn. Magn. Mat.* **170**, 253 1997.
26. B. Velicky, S. Kirkpatrick, and H. Ehrenreich, *Phys. Rev.* **175**, 747 1968.
27. H. J. Leder and G. Czycholl, *Z. Phys. B* **35**, 7 1979.
28. R. Martin and J. W. Allen, *J. Appl. Phys.* **50**(11), 7561 1979.
29. G. Czycholl, *Physics Reports* **143**(5), 277 1986.
30. T. Herrmann and W. Nolting, *Phys. Rev. B* **53**(16), 10579 1996.
31. T. Pruschke, M. Jarrell, and J. K. Freericks, *Adv. Phys.* **44**(2), 187 1995.
32. A. Georges, G. Kotliar, W. Krauth, and M. J. Rozenberg, *Rev. Mod. Phys.* **68**(1), 13 1996.
33. W. Metzner and D. Vollhardt, *Phys. Rev. Lett.* **62**, 324 1989.
34. E. Müller-Hartmann, *Z. Phys. B* **74**, 507 1989.
35. M. Potthoff, T. Wegner, and W. Nolting, *Phys. Rev. B* **55**(24), 16132 1997.
36. D. Meyer, T. Wegner, M. Potthoff, and W. Nolting, *Physica B* **270**, 225 1999.
37. A Martin-Rodero, F. Flores, M. Baldo, and R. Pucci, *Solid State Commun.* **44**, 911 1982.
38. A Martin-Rodero, E. Louis, F. Flores, and C. Tejedor, *Phys. Rev. B* **33**, 1814 1986.
39. H. Kajueter and G. Kotliar, *Phys. Rev. Lett.* **77**(1), 131 1996.
40. K. Yamada, *Prog. Theo. Phys.* **53**, 970 1975.
41. V. Zlatič and B. Horvatič, *Phys. Rev. B* **28**(12), 6904 1983.
42. A. Levy Yeyati, A. Martin-Rodero, and F. Flores, *cond-mat/9910190* 1999.
43. O. Takagi and T. Saso, *J. Phys. Soc. Japan* **68**(9), 2894 1999.
44. N. S. Vidhyadhiraja, A. N. Tahvildar-Zadeh, M. Jarrell, and H. R. Krishnamurthy, *Europhys. Lett.* **49**(4), 459 2000.
45. J. M. Luttinger and J. C. Ward, *Phys. Rev.* **118**(5), 1417 1960.
46. J. Friedel, *Can. J. Phys.* **34**, 1190 1956.
47. D. Langreth, *Phys. Rev.* **150**(2), 516 1966.
48. T. Saso, *Physica B* **281&282**, 315 2000.
49. M. Potthoff, T. Herrmann, T. Wegner, and W. Nolting, *phys. stat. sol. (b)* **210**, 199 1998.
50. M. C. Gutzwiller, *Phys. Rev. Lett.* **10**(5), 159 1963.
51. J. Kanamori, *Prog. Theor. Phys* **30**, 275 1963.
52. M. Ulmke, *Eur. Phys. J. B* **1**, 301 1998.
53. T. Obermeier, T. Pruschke, and J. Keller, *Phys. Rev. B* **56**(4), R8479 1997.
54. D. Vollhardt, N. Blümer, K. Held, M. Kollar, J. Schlipf, and M. Ulmke, *Z. Phys. B* **103**, 283 1997.
55. T. Herrmann and W. Nolting, *Solid State Commun.* **103**(6), 351 1997.
56. J. Wahle, N. Blümer, J. Schlipf, K. Held, and D. Vollhardt, *Phys. Rev. B* **58**, 12749 1998.